Adaptive Super-resolution for Ocean Bathymetric Maps using a Deep Neural Network and Data Augmentation

Koshiro Murakami[1], Daisuke Matsuoka[1], Naoki Takatsuki[2], Mitsuko Hidaka[1], Yukari Kido[1] and Eiichi Kikawa[1, 2]

[1]Japan Agency for Marine-Earth Science and Technology (JAMSTEC), Yokohama, Japan.

[2]IDEA Consultants, Inc., Yokohama, Japan.

Corresponding author: Daisuke Matsuoka (daisuke@jamstec.go.jp)

Key Points:

- Adaptive data augmentation improved bathymetric super-resolution, achieving RMSE reduction of up to 14.3% in a finer mapping mesh.
- The two-step data augmentation method overcomes feature dissimilarity limitations in supervised machine learning for enhanced map details.
- The proposed method enables application of image super-resolution to data-scarce areas, thus facilitating bathymetric research.

Abstract

Machine learning-based image super-resolution is a robust approach for obtaining detailed bathymetric maps. However, in machine learning using supervised data, the dissimilarity in the features of training and target datasets degrades super-resolution performance. This study proposes a two-step method to generate training data with features similar to those of the target data using image transformation and composition. The super-resolution model trained via the proposed method on the Central Okinawa Trough data was applied to the bathymetry data around Okinotorishima Islands. The method improved the root mean squared error by up to 14.3% compared to conventional approaches, thus demonstrating the potential of combining artificial data generation with machine learning for super-resolution bathymetry mapping of the entire ocean floor.

Plain Language Summary

Mapping the ocean floor in high detail is crucial for research and conservation, but traditional methods can be expensive and limited. This study tackled a key challenge in using machine learning to create detailed seabed maps: the mismatch between training data and real-world conditions. We developed a new method that "invents" training data similar to the target area by cleverly manipulating existing data. This allowed us to create maps with twice the resolution of previous methods, even when starting with limited data. This breakthrough opens the door to creating highly detailed maps of underwater features anywhere in the world, aiding scientists in understanding and protecting our precious oceans.

1 Introduction

High-resolution seafloor bathymetric maps are essential for geomorphology, physical oceanography, and marine biodiversity studies as well as for resource management and disaster prevention. A recent report highlighted that only about 24.9% of the entire seafloor has been mapped in detail using acoustic surveys (https://seabed2030.org/2023/05/02/hsh-prince-albert-ii-of-monaco-announces-a-quarter-of-the-ocean-now-mapped/). Obtaining an accurate global bathymetric map is one of the most important scientific challenges being addressed through the ongoing international project “The Nippon Foundation-GEBCO Seabed 2030”, aimed at collecting 100% of detailed seafloor topographic maps by 2030 (Mayer et al., 2018).

Acoustic bathymetry is costly and time consuming; therefore, obtaining complete global seabed maps by 2030 with this method alone would not be realistic. Supplementing acoustic observations with a machine-learning-based super-resolution technique could be a viable approach (e.g. Lepcha et al., 2023). Improving low-resolution bathymetry data with numerical methods could be instrumental for achieving the goals of Seabed 2030. In the past, mathematical interpolation methods such as splines (Briggs, 1974; Nock et al., 2019) and geostatistical methods (Deutsch and Journel, 1998; Chilès and Delfiner, 2012), have been used. Machine-learning-based approaches have also been attempted, including super-resolution methods based on neural networks (Koike et al., 2002; Koike and Matsuda, 2003) and sparse coding (Yang et al., 2010; Yutani et al., 2022). In recent years, several researchers utilized deep convolutional neural networks and proposed super-resolution methods for bathymetric mapping (Sonogashira et al., 2020; Hidaka et al., 2021; Li et al., 2022; Cai et al., 2023). Deep learning-based super-resolution methods have attracted attention because of their enhanced accuracy compared to conventional methods and have been used in geophysics research fields (e.g. Yasuda et al. 2022; Kuehn et al. 2023; Liu et al. 2024).

However, the approach using supervised machine learning sometimes degrades performance for the data with features different from those of a training dataset. Therefore, when a super-resolution model trained with the data from one area is applied to another ocean area, the performance degradation might be inevitable. Data augmentation artificially generates new data by modifying existing data through geometric transformations and color adjustments to compensate for the lack of training data in machine learning (Shorten and Khoshgoftaar, 2019). These methods have effectively improved accuracy in many cases when training data are limited. However, while data augmentation generates new data, it often suffers from limited feature diversity, hindering performance in real-world scenarios with unseen features.

Therefore, in this study, we attempted to improve super-resolution performance by artificially generating data with features similar to those of a target test area. This artificial data generation was achieved by combining two types of bathymetric maps with different features. To validate the effectiveness of the proposed method, we used bathymetric data from the Central Okinawa Trough as training data and performed 4-fold super-resolution from a 50-m to 12.5-m mesh on data around Okinotorishima Islands, which had different features. The validity of the

proposed method was confirmed by comparing the super-resolution results with those obtained using several data augmentation methods.

2 Materials

We designed a case study to demonstrate the effectiveness of the proposed super-resolution method, using bathymetry data from two different oceanographic regions: the target dataset for model validation from the Okinotorishima area and the training dataset for model development from the Okinawa Trough.

2.1 Bathymetric map around Okinotorishima Islands for target data

Okinotorishima Islands are the southernmost of Japan's islands, located 1,700 km south of Tokyo. The Ministry of Land, Infrastructure, Transport and Tourism, the Ministry of Economy, Trade and Industry (MILT), the Ministry of Agriculture, Forestry and Fisheries (MAFF), and the Tokyo Metropolitan Government (TMG) have continuously worked together to understand the unique biodiversity and conserve marine resources of Okinotorishima Islands, since the islands are remote and isolated. The Geological Survey of Japan conducted dredging on the slopes of the islands recovering islands' base igneous rocks and overlying limestone samples in 1989. The bathymetric data for the surrounding area was published by the Japan Coast Guard Hydrographic Department (1991) as a 1:50,000 bathymetric map developed from geophysical surveys in 1991.

From August 14th to 25th, 2022, a bathymetric survey was conducted aboard research vessel Kaiyo Maru No. 2 (Kaiyo Engineering Co., Ltd.) using a multibeam echosounder (MBES). A 10-m mesh bathymetric mapping survey was conducted for the island areas shallower than 2,000 m. For the areas with depths ranging from 950 to 1,450 m, autonomous underwater vehicle (AUV) observations were conducted on three lines on the northern slopes of the islands. The obtained 3D point cloud data was converted to 100-m mesh and 25-m mesh

grids through integration and correction processes. The Okinotorishima Islands are surrounded by steep slopes, as seen in the bathymetric map in Figure 1 (a).

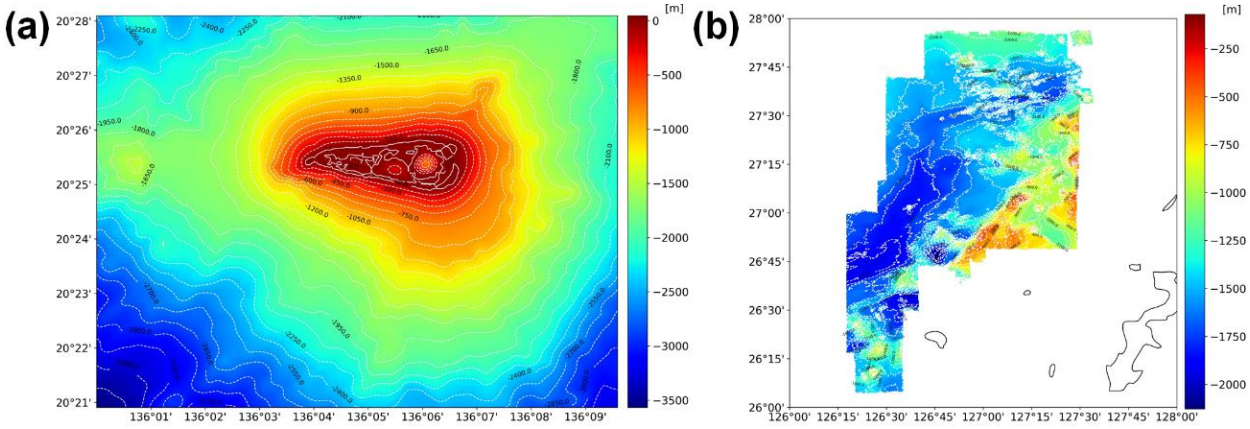

Figure 1. Bathymetric maps used in this study. Data around (a) the Okinotorishima Islands for training the super-resolution model and (b) the Mid-Okinawa Trough for evaluating the model performance.

2.2 Bathymetric map of the Okinawa Trough for training data

We used the bathymetry data from the Mid-Okinawa Trough as the training dataset. The Central Okinawa Trough, shown in Figure 1 (b), is known as an important research area rich in geological resources; previous surveys have revealed several submarine volcanoes and high hydrothermal activity areas (Kasaya et al., 2015; Nakamura et al., 2015).

The data were obtained from a MBES survey in 2014. Integration and correction processes were performed on the obtained bathymetric point cloud data, which were interpolated into 100-m and 25-m grids (Kasaya et al., 2020). In the study by Hidaka et al. (2021) and Yutani et al. (2022), the high-resolution data after super-resolution were obtained from a 100-m mesh, whereas in the current study, the mesh size was set to 50 m to match the resolution of the target data.

3 Methods

3.1 Super-resolution using a deep neural network

The Efficient Sub-Pixel Convolutional Neural Network (ESPCN), a deep neural network architecture described by Shi et al. (2016), was trained to achieve a 4-fold increase in resolution. To increase the resolution of the bathymetric map four-fold within an area of approximately 800

129 square meters, the size of the input and output layer of the super-resolution model was 16×16
130 and 64×64 pixels, respectively.
131 Spatial patterns are extracted by applying several convolution operations to the input low-
132 resolution image. A sub-pixel convolution layer, which performs inverse convolution
133 (deconvolution) before the output layer, is placed to expand the image to the target resolution.
134 Generally, the deconvolution process to increase the resolution may cause lattice noise, but
135 ESPCN overcomes this issue by the operation called Pixel Shuffle. Compared with other deep
136 learning-based super-resolution architectures, such as a SRCNN (Dong et al., 2014), FSRCNN
137 (Dong et al., 2016), SRGAN (Ledig et al., 2017), and ESRGAN (Wang et al., 2019), ESPCN
138 offers a well-balanced trade-off between accuracy, learning stability, and speed. Thus, the
139 ESPCN model was employed in this study, but the proposed method can be applied to other
140 super-resolution network architectures.
141 In this work, we evaluated super-resolution results using two common metrics, root mean
142 squared error (RMSE) and peak signal-to-noise ratio (PSNR), using Equation (1).

143 $$PSNR = 10 \cdot \log_{10} \frac{MAX_I^2}{MSE} \quad (1)$$

144 where, MAX_I is the maximum value that the pixel value can take and MSE is the mean squared
145 error.
146 In this study, pixel values were normalized to the range of 0 to 1, where $MAX_I = 1$. While
147 PSNR is a suitable metric for evaluating the quality of bathymetric images overall, it cannot
148 accurately capture areas with sharp changes in depth. Therefore, in this study, we also used
149 RMSE, which is an evaluation index generally used in machine learning. The RMSE is the

square root of the MSE, which is the square of an error between the true value and super-resolution result at each pixel averaged over the entire image, calculated using Equation (2).

$$RMSE = \sqrt{\frac{1}{mn}\sum_{i=1}^{m}\sum_{j=1}^{n}\left(x_{i,j} - y_{i,j}\right)^2} \quad (2)$$

where, i and j are the pixel positions, m and n are the image width and height, x is the super-resolution image (output image), and y is the high-resolution image (ground truth image).

3.2 Adaptive data augmentation

We propose an adaptive data augmentation method specifically designed for super-resolution of target data with characteristics different from those of training data. Using a two-step process of data augmentation and sampling, we generated training data similar to the target data (Figure 2). Data augmentation increases the amount of training data and reduces inference errors by transforming existing data (Shorten and Khoshgoftaar, 2019). The proposed method combines multiple data augmentation methods: image flipping, rotation, and mixup for diverse training samples.

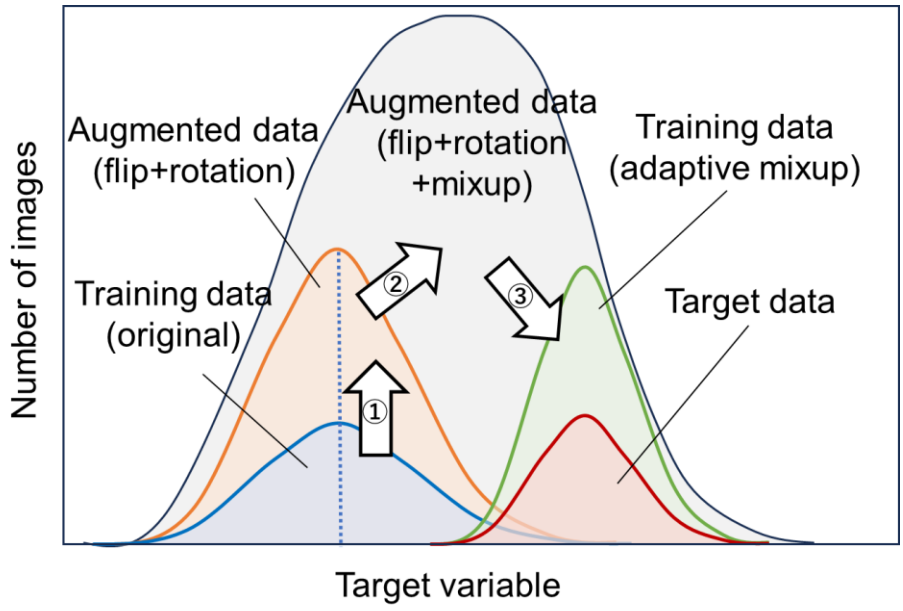

Figure 2. Conceptual diagram of adaptive data augmentation.

Image flipping and rotation increase the number of data frames by applying geometric transformations while maintaining the characteristics of the original image. Image flipping can

be vertical (upside down) or horizontal (mirror image). By applying the horizontal flip to the result of the vertical flip, four images are generated from a single source image. Image rotation transforms the source image into a different image by rotating it to an arbitrary angle. In our study, new images were generated by rotating the original image from 30 to 330 degrees in increments of 30. The original image, designated as zero-degree rotation, and 180 degree rotation were excluded because of overlap with the vertical and horizontal flipping. The missing wedges due to rotation were filled by reflection from the original image. By applying rotation to the flipping result, one original image was replicated 40 times. These methods of geometrical transformation were used by Sonogashira et al. (2020) to artificially increase the training dataset. They have also been used in natural science fields, such as meteorological and medical imaging, to improve accuracy (Matsuoka et al., 2021; Kalaivani et al., 2023).

Image flipping and rotation only changes the orientation of the image, not topographic parameters such as slope or gradient, but mixup represents a data augmentation method that generates new data from two different images (Zhang et al., 2018). In this study, mixup was applied to the flipped-and-rotated results to artificially change topographic quantities. The mixup is mathematically represented by Equations (3) and (4).

$$\tilde{x} = \lambda x_i + (1-\lambda)x_j \quad (3)$$

$$\tilde{y} = \lambda y_i + (1-\lambda)y_j \quad (4)$$

were, x_i and x_j indicate a low-resolution image randomly sampled from data where some target physical quantity is lower and higher than the median of the training data, respectively (similarly, y_i and y_j indicate a high-resolution image); a parameter, $\lambda \in [0, 1]$, determines the ratio of mixing two different types of data; $\tilde{x}$ and $\tilde{y}$ are the low- and high-resolution images after mixup, respectively.

Next, the data generated by flipping and rotation were divided into two groups, bounded by an appropriate threshold of a targeted physical quantity. By sampling data from both groups one at a time and applying a mixup with appropriate weights λ, new pairs of high-resolution $\tilde{x}$ and low-resolution $\tilde{y}$ images were obtained.

By sampling from flipped and mixed-up images, we generated training data with features similar to those of the test dataset. Here, we aimed for an ideal training set with an *n*-times higher frequency distribution compared to the test data. We randomly selected samples from the mixed-up data that fell within *n* times the target data's frequency distribution. This ensured that these

199 samples closely resembled the test data; dissimilar samples were discarded. This selection
200 process continued until all augmented data were explored, resulting in a training set closely
201 matching the target frequency distribution.
202
203 **4 Results and Discussion**
204 4.1 Training super-resolution model using adaptive data augmentation
205 The proposed method was applied to the bathymetry data of the Okinawa Trough to
206 adaptively generate training data with features similar to the bathymetry data of Okinotorishima
207 Islands. The mean slope gradient (MSG), which indicates the average of slope gradient within an
208 arbitrary region, was selected as the target variable. The slope gradient (SG) is defined as the
209 mean elevation of neighboring eight grids with each grid in the image as follows (Equations 5
210 and 6).

211 $$S_x = \frac{H_{i+1,j-1} + H_{i,j-1} + H_{i-1,j-1} - \left(H_{i+1,j+1} + H_{i,j+1} + H_{i-1,j+1}\right)}{6D_x} \quad (5)$$

212 $$S_y = \frac{H_{i+1,j-1} + H_{i+,j} + H_{i+1,j+1} - \left(H_{i-1,j-1} + H_{i-1,j} + H_{i-1,j+1}\right)}{6D_y} \quad (6)$$

213 $$SG = \sqrt{{S_x}^2 + {S_y}^2} \quad (7)$$

214 where, $\boldsymbol{H_{i,j}}$ is the water depth at position $(\boldsymbol{i,j})$; *i* and *j* are the index number in the x- and y-
215 direction in 2-dimensional space; and $\boldsymbol{D_x}$ and $\boldsymbol{D_y}$ are the distances between the grids in the x and
216 y directions, respectively.
217 In this study, we defined MSG as the average amount of seabed SG within an 800 m^2
218 area (256×256 grids for high resolution and 64×64 grids for low resolution), which represented
219 the basic unit in both training and testing. Research has shown that super-resolution accuracy
220 decreases as terrain SG increases (Hidaka et al., 2021).
221 First, we separated the bathymetry image of the Okinawa Trough into small regions. The
222 number of grids for the small-area images was 64×64 grids for high resolution and 16×16 grids
223 for low resolution, each with 11,053 images. Next, we proceeded with data augmentation by

flipping and rotating original images. The number of images at this point was 154,742, which is 14 times the amount of the original data.

Examples of images produced by mixup are shown in Figure 3 (a). In the first row, one image was selected from each of the groups with large and small MSG, and mixup was applied (weight $\lambda = 0.3$) to the image with the largest slope. The MSG values of the large and small MSG groups were 0.359 and 0.009, respectively; the tilt of the generated image was 0.108. A histogram of the data generated by the adaptive mixup for each MSG is shown in Figure 3 (b). Image flipping and rotating simply increases the amount of original training data, which is not

sufficient for the data with a large MSG. However, the combination with mixup succeeded in increasing the amount of data with a large MSG.

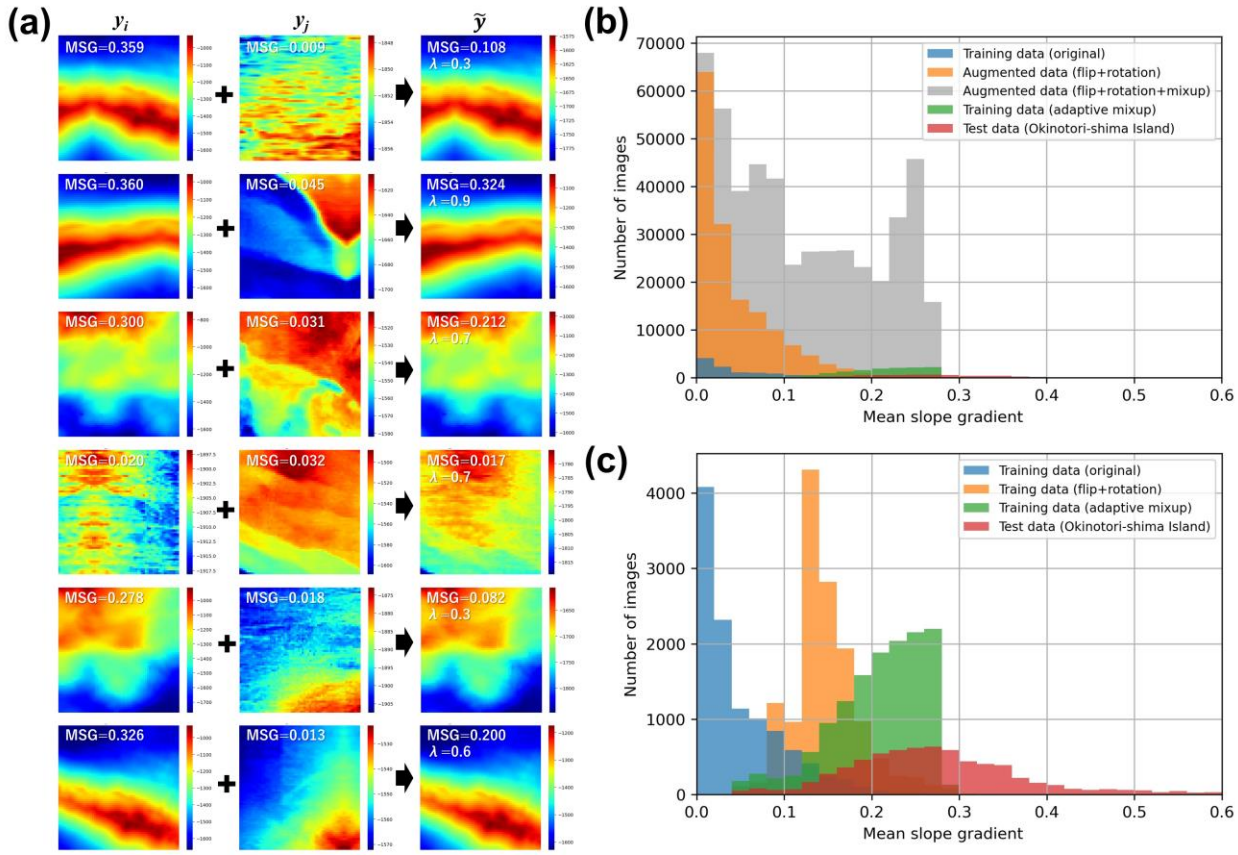

Figure 3. Data augmentation results using adaptive mixup. (a) Resultant images and numbers of images (b) before and (c) after adaptive mixup, where MSG is the mean slope gradient of the image.

To validate the effectiveness of the proposed method, we trained the super-resolution model on three different training datasets, as shown in Figure 3 (c), and compared the results. The first training set included original data and the second set included the flipped-and-rotated data, sampled as close as possible to the histogram of the target data. The third dataset was

sampled from a mixup data, as close as possible to the histogram of the target data. Both data augmentation methods were applied to double the original data for fair comparison.

4.2 Performance evaluation

We evaluated the super-resolution model trained with three different datasets on Okinotorishima Islands data. Figure 4 shows the PSNR and RMSE of the MSG for each output image. The proposed method model surpassed the original model for most MSG ranges (0.1–0.3) with adaptively increased data. For example, the proposed method achieved a mean PSNR of 57.94 dB for MSG 0.2–0.22, compared to the original model's 57.50 dB. In the range of MSG greater than 0.14, where the amount of data generated by the proposed method exceeded the original data, the RMSE improved by 14.3% (RMSE of the flip + rotation model improved by 7.2%). Although the target dataset was small, the RMSE also improved by 33.0% in the MSG range of 0.06–0.08, where the effect of adaptive data augmentation was minimal. In cases of MSG less than 0.38, the accuracy of the proposed method was equal to or higher than that of the original; however, for MSG exceeding 0.38 (the maximum value), the adaptive model showed a lower accuracy than the original, in terms of both PSNR and RMSE. While this range has a

minor target data impact on the overall area, it should be noted when processing steep-slope topographic data.

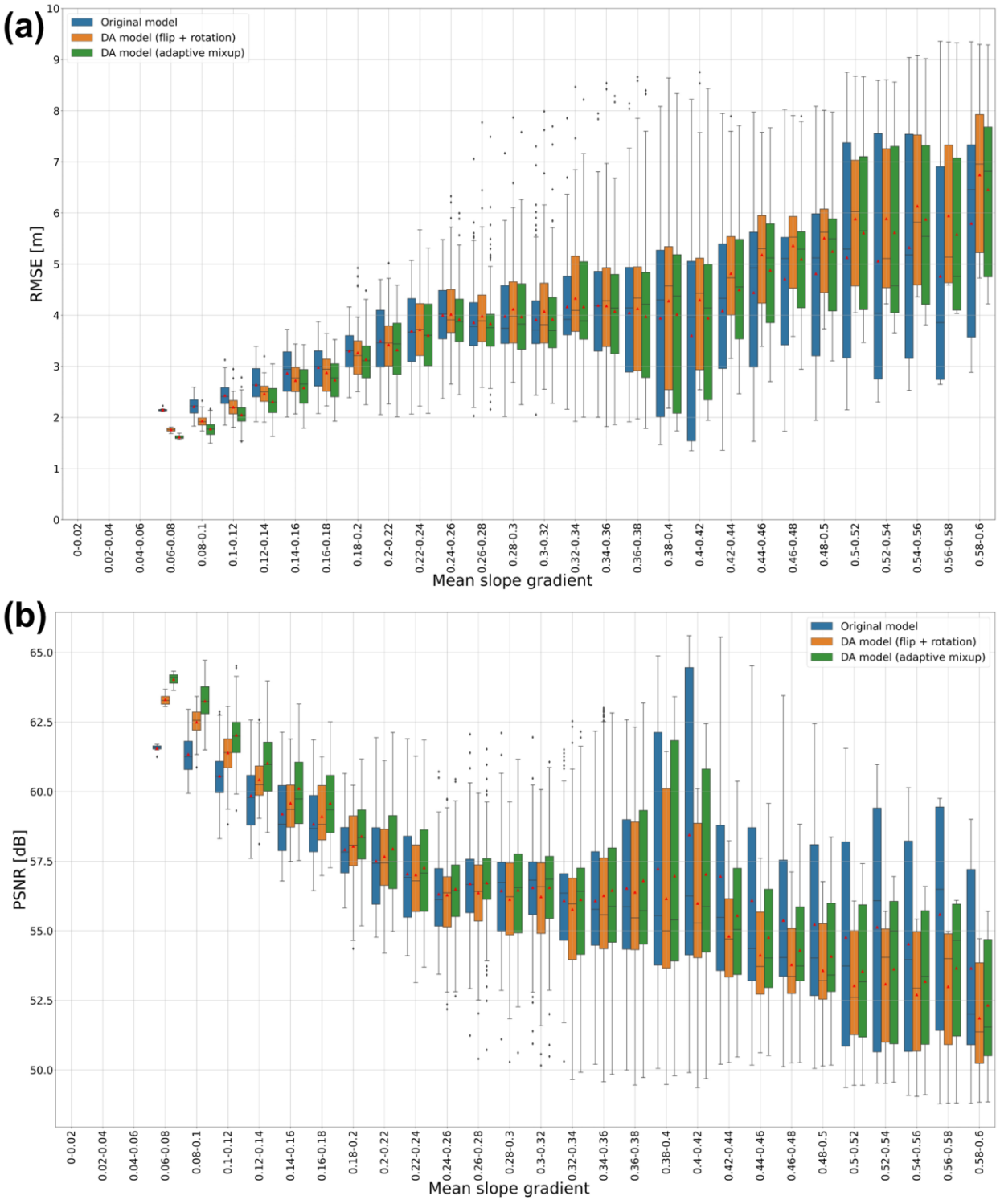

Figure 4. The super-resolution performance of (a) RMSE and (b) PSNR applied to the Okinotorishima Islands bathymetry data. Comparisons between three models trained using original, flipped-and-rotated, and adapted data.

A spatial comparison of the super-resolution performance of the original and adaptive models is shown in Fig. 5. Figure 5 (a) illustrates the effect of subtracting the PSNR of the proposed model from the PSNR of the original model. The results are positive when the adaptive model is superior and negative when it is inferior. Figure 5 (b) shows the distribution of the MSG in a region with 256 grid squares, centered on each grid. The original model showed a better PSNR than the adaptive model, especially in the vicinity of the island, where the seabed was steep, with MSG exceeding 0.4. However, away from the island, the adaptive model

outperformed the original model in the areas with gradual MSG less than 0.4; both models showed a similar accuracy in areas where the MSG exceeded 0.4.

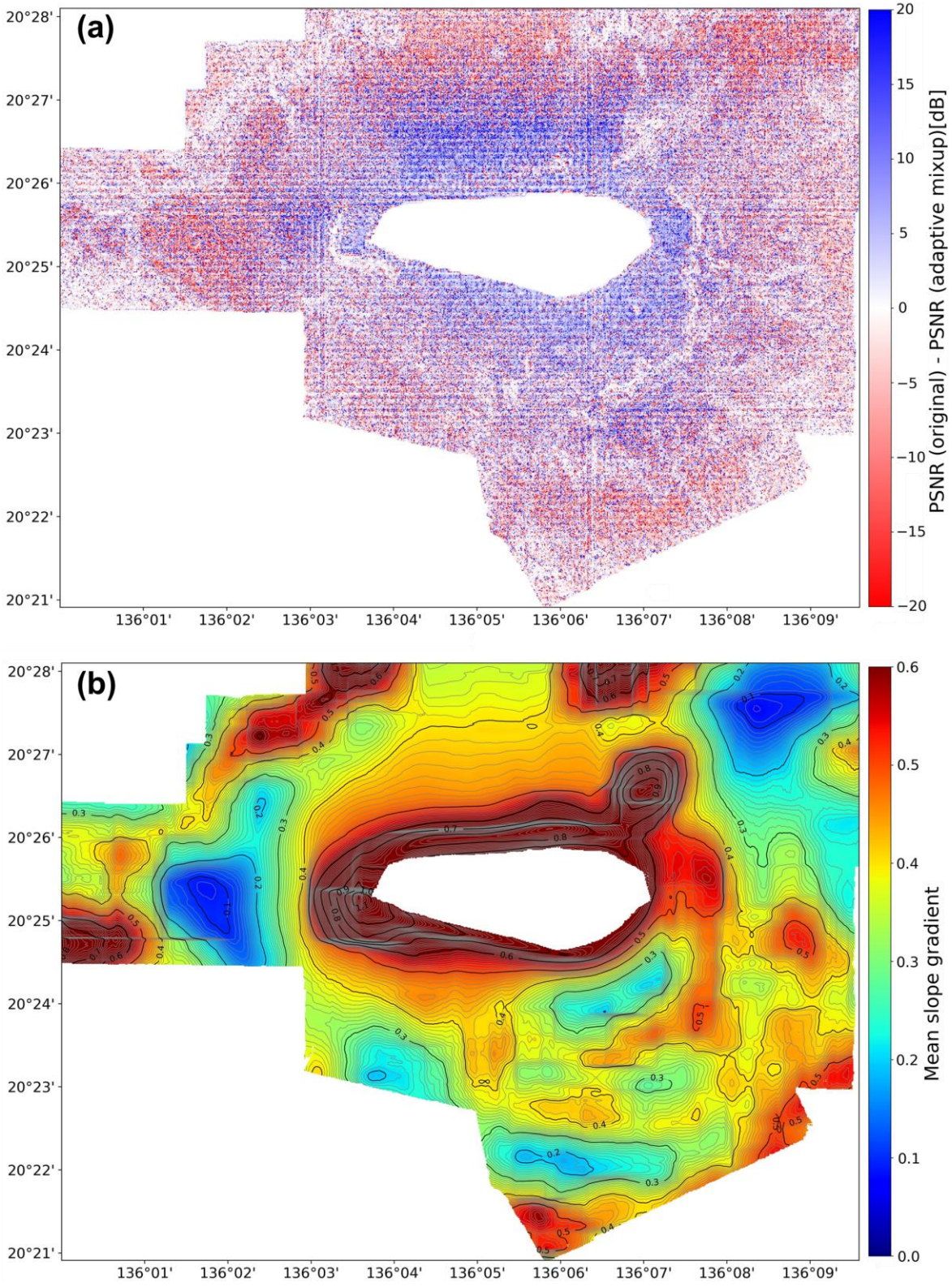

Figure 5. Comparison of the spatial distribution of super-resolution performance (PSNR) between the original model and the proposed method. (a) Difference in PSNR between original and adaptive models and (b) spatial distribution of the mean slope gradient.

4.3 Limitations and future work

The proposed adaptive mixup method relies on existing bathymetry data, limiting its ability to generate data for all features. For example, the maximum MSG generated in this case study was 0.3 (Figs. 3 (b) and (c)), with no data above that range. This lack of data likely contributed to the performance limitations in regions with a higher MSG, where artificially generated data were not sufficient. In the area with an MSG range of 0.22–0.28, there was no advantage of the proposed method, despite the sufficient amount of data. This may be due to a lack of data for values above 0.28, which may have affected the super-resolution performance in that range. Similarly, the lower accuracy of the original model for low MSG values (0.04–0.12) might be due to its specialization for flat terrain. It is important to analyze the similarities of the features between the target data and the optimal training data to achieve the best performance.

In theory, it is possible to intentionally generate characteristic data by using extremely large values as weights during mixup or by scaling data up or down vertically or horizontally. However, in such cases, the geomorphological validity of the data may be lost. Our future work will explore generating characteristic data using methods such as generative adversarial networks (GANs) or data augmentation with geomorphological constraints, while ensuring data validity.

5 Conclusions

This study introduced an adaptive machine learning method that applies the super-resolution model to a seabed area with characteristics different from those of the training data. The proposed method, involving a two-stage augmented training data generation, demonstrated improved super-resolution accuracy compared to the original model. However, its application is currently limited to terrains that can be effectively generated based on real data. We are actively exploring methods of data generation independent of real data to extend the applicability of this method to any terrain globally.

Acknowledgments

We are grateful to Dr. T. Kuwatani, J. Kaneko and T. Kasaya for the helpful discussions. This research was partly supported by the Tokyo Metropolitan Government.

Open Research Statement

Bathymetry data are available at Data and Sample Research System for Whole Cruise Information (DARWIN) (https://www.godac.jamstec.go.jp/darwin_tmp/explain/81/e/) and IHO Data Centre for Digital Bathymetry (DCDB) (https://www.ncei.noaa.gov/maps/iho_dcdb/). The source code for super-resolution and data augmentation is available upon request.

References

Briggs, I. C. (1974) Machine contouring using minimum curvature. *Geophysics*, 39:1, 39–48. https://doi.org/10.1190/1.1440410

Cai, W., Liu, Y., Chen, Y., Dong, Z., Yuan, H. & Li, N. (2023). A seabed terrain feature extraction transformer for the super-resolution of the digital bathymetric model. *Remote Sensing*, 15(20), 4906. https://doi.org/10.3390/rs15204906

Chilès, J.-P. & Delfiner, P. (2012). Geostatistics: Modeling Spatial Uncertainty 2nd Edition. New York, NY: Wiley.

Deutsch, C. V. & Joumel, A. G. (1998). GSLIB Geostatistical Software Library and User's Guide 2nd edition. New York, NY: Oxford University Press.

Dong, C., Loy, C. C., He, K. & Tang, X. (2014). Learning a deep convolutional network for image super-resolution. Paper presented at European Conference on Computer Vision (ECCV) 2014, Zurich, Switzerland.

Dong, C., Loy, C. C. & Tang, X. (2016). Accelerating the super-resolution convolutional neural network. Paper presented at European Conference on Computer Vision (ECCV) 2014, Zurich, Switzerland.

Kalaivani, S., Asha, N., & Gayathri, A. (2023). Geometric Transformations-Based Medical Image Augmentation. In: Solanki, A. & Naved, M. (eds), *GANs for Data Augmentation in Healthcare* (pp.133-141). Cham, Switzerland: Springer International Publishing.

Kasaya, T., Machiyama, H., Kitada, K. & Nakamura, K. (2015). Trial exploration for hydrothermal activity using acoustic measurements at the North Iheya Knoll. *Geochemical Journal*, 49(6), 597–602. https://doi.org/10.2343/geochemj.2.0389

Kasaya, T., Kaneko, J. & Iwamoto, H. (2020). Observation and confirmation based on survey protocol for seafloor massive sulfide deposits using acoustic survey technique and self-potential surveys. *BUTSURI-TANSA*, 73, 42–52. https://doi.org/10.3124/segj.73.42

Hidaka, M., Matsuoka, D., Kuwatani, T., Kaneko, J., Kasaya, T., Kido, Y., Ishikawa, Y. & Kikawa, E. (2021). Super-resolution for ocean bathymetric maps using deep learning approaches: A comparison and validation. *Geoinformatics*, 32(1), 3–13. https://doi.org/10.6010/geoinformatics.32.1_3

Koike, K., Matsuda, S., Suzuki, T. & Ohmi, M. (2002). Neural network-based estimation of principal metal contents in the Hokuroku District, northern Japan, for exploring kuroko-type deposits. *Natural Resources Research*, 11, 135–156. https://doi.org/10.1023/A:1015520204066

Koike, K. & Matsuda, S. (2003). Characterizing content distributions of impurities in a limestone mine using a feedforward neural network. *Natural Resources Research*, 12, 209–223, https://doi.org/10.1023/A:1025180005454

Kuehn, J., Abadie, S., Liquet, B., & Roeber, V. (2023). A deep learning super-resolution model to speed up computations of coastal sea states. *Applied Ocean Research*, 141, 103776. https://doi.org/10.1016/j.apor.2023.103776

Ledig, C., Theis, L., Huszár, F., Caballero, J., Cunningham, A., Acosta, A., Aitken, A., Tejani, A., Totz, J., Wang, Z. & Shi, W. (2017). Photo-realistic single image super-resolution using a generative adversarial network. Paper presented at IEEE Conference on Computer Vision and Pattern Recognition (CVPR) 2017, Honolulu, HI.

Lepcha, D. C., Goyal, B., Dogra, A., & Goyal, V. (2023). Image super-resolution: A comprehensive review, recent trends, challenges and applications. *Information Fusion*, 91, 230–260. https://doi.org/10.1016/j.inffus.2022.10.007

Li, X., Li, J., Williams, Z., Huang, X., Carroll, M., Wang, J. (2023). Enhanced deep learning super-resolution for bathymetry data. Paper presented at 2022 IEEE/ACM International Conference on Big Data Computing, Applications and Technologies (BDCAT), Vancouver, Canada.

Liu, B., Ning, X., Ma, S., & Yang, Y. (2024). Multi-scale dense spatially-adaptive residual distillation network for lightweight underwater image super-resolution. *Frontiers in Marine Science*, 10, 1328436. https://doi.org/10.3389/fmars.2023.1328436

Matsuoka, D. (2021). Classification of imbalanced cloud image data using deep neural networks: Performance improvement through a data science competition. *Progress in Earth and Planetary Science*, 8. https://doi.org/10.1186/s40645-021-00459-y

Mayer, L., Jakobsson, M., Allen, G., Dorschel, B., Falconer, R., Ferrini, V., Lamarche, G., Snaith, H. & Weatherall, P. (2018). The Nippon Foundation—GEBCO Seabed 2030 Project: The quest to see the world's oceans completely mapped by 2030. *Geosciences*, 8(2), 63. https://doi.org/10.3390/geosciences8020063

Nakamura, K., Kawagucci, S., Kitada, K., Kumagai, H., Takai, K. & Okino, K. (2015). Water column imaging with multibeam echo-sounding in the Mid-Okinawa Trough: Implications for distribution of deep-sea hydrothermal vent sites and the cause of acoustic water column anomaly. *Geochemical Journal*, 49(6), 579–596. https://doi.org/10.2343/geochemj.2.0387

Nock, K., Bonanno, D., Elmore, P., Smith, L., Ferrini, V. & Petry, F. (2019). Applying single-image super-resolution for the enhancement of deep-water bathymetry. *Heliyon*, 5, e02570. https://doi.org/10.1016/j.heliyon.2019.e02570

Shi, W., Caballero, J., Huszár, F., Totz, J., Aitken, A. P., Bishop, R., Rueckert, D. & Wang, Z. (2016). Real-time single image and video super-resolution using an efficient sub-pixel convolutional neural network. Paper presented at IEEE Conference on Computer Vision and Pattern Recognition (CVPR) 2016, Las Vegas, NV.

Shorten, C., Khoshgoftaar & T. M. (2019). A survey on image data augmentation for deep learning. *Journal of Big Data*, 6, 60. https://doi.org/10.1186/s40537-019-0197-0

Sonogashira, M., Shonai, M. & Iiyama, M. (2020). High-resolution bathymetry by deep-learning-based image super resolution. *PLoS ONE*, 15(7), e0235487. https://doi.org/10.1371/journal.pone.0235487

Yang, J., Wright, J., Huang, T. & Ma, Y. (2010). Image super-resolution via sparse representation. *IEEE Transactions on Image Processing*, 19(11), 2861–2873. https://doi.org/10.1109/TIP.2010.2050625

Yasuda, Y., Onishi, R., Hirokawa, Y., Kolomenskiy, D. & Sugiyama, D. (2022). Super-resolution of near-surface temperature utilizing physical quantities for real-time prediction of urban micrometeorology. *Building and Environment*, 209, 108597. https://doi.org/10.1016/j.buildenv.2021.108597

Yutani, T., Yono, O., Kuwatani, T., Matsuoka, D., Kaneko, J., Hidaka, M., Kasaya, T., Kido, Y., Ishikawa, Y., Ueki, T. & Kikawa, E. (2022). Super-resolution and feature extraction for ocean bathymetric maps using sparse coding. *Sensors*, 22(9), 3198. https://doi.org/10.3390/s22093198

Wang, X., Yu, K., Wu, S., Gu, J., Liu, Y., Dong, C., Qiao, Y. & Loy, C. C. (2019). ESRGAN: Enhanced super-resolution generative adversarial networks. Paper presented at European Conference on Computer Vision (ECCV) 2019, Munich, Germany.

Zhang, H., Cisse, M., Dauphin, Y. N. & Lopez-Paz, D. (2018). mixup: Beyond empirical risk minimization. Paper presented at International Conference on Learning Representation (ICLR) 2018, Vancouver, Canada.

Figure 1.

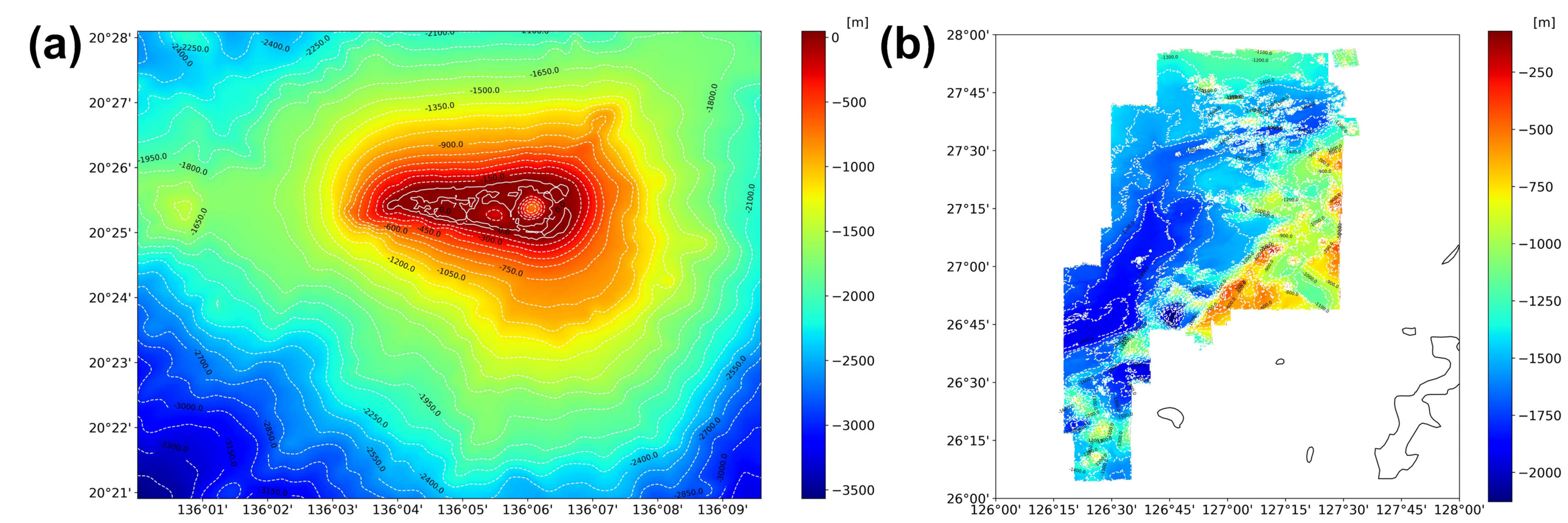
(a)
20°28'
20°27'
20°26'
20°25'
20°24'
20°23'
20°22'
20°21'
136°01'
136°02'
136°03'
136°04'
136°05'
136°06'
136°07'
136°08'
136°09'
[m]
0
−500
−1000
−1500
−2000
−2500
−3000
−3500
(b)
28°00'
27°45'
27°30'
27°15'
27°00'
26°45'
26°30'
26°15'
26°00'
126°00'
126°15'
126°30'
126°45'
127°00'
127°15'
127°30'
127°45'
128°00'
[m]
−250
−500
−750
−1000
−1250
−1500
−1750
−2000

Figure 2.

Augmented data
(flip+rotation)

Augmented data
(flip+rotation
+mixup)

Training data
(adaptive mixup)

Training data
(original)

Test data

①

②

③

Number of images

Target variable

Figure 3.

(a)

y_i y_j $\tilde{y}$

MSG=0.359 MSG=0.009 MSG=0.108 λ =0.3

MSG=0.360 MSG=0.045 MSG=0.324 λ =0.9

MSG=0.300 MSG=0.031 MSG=0.212 λ =0.7

MSG=0.020 MSG=0.032 MSG=0.017 λ =0.7

MSG=0.278 MSG=0.018 MSG=0.082 λ =0.3

MSG=0.326 MSG=0.013 MSG=0.200 λ =0.6

(b)

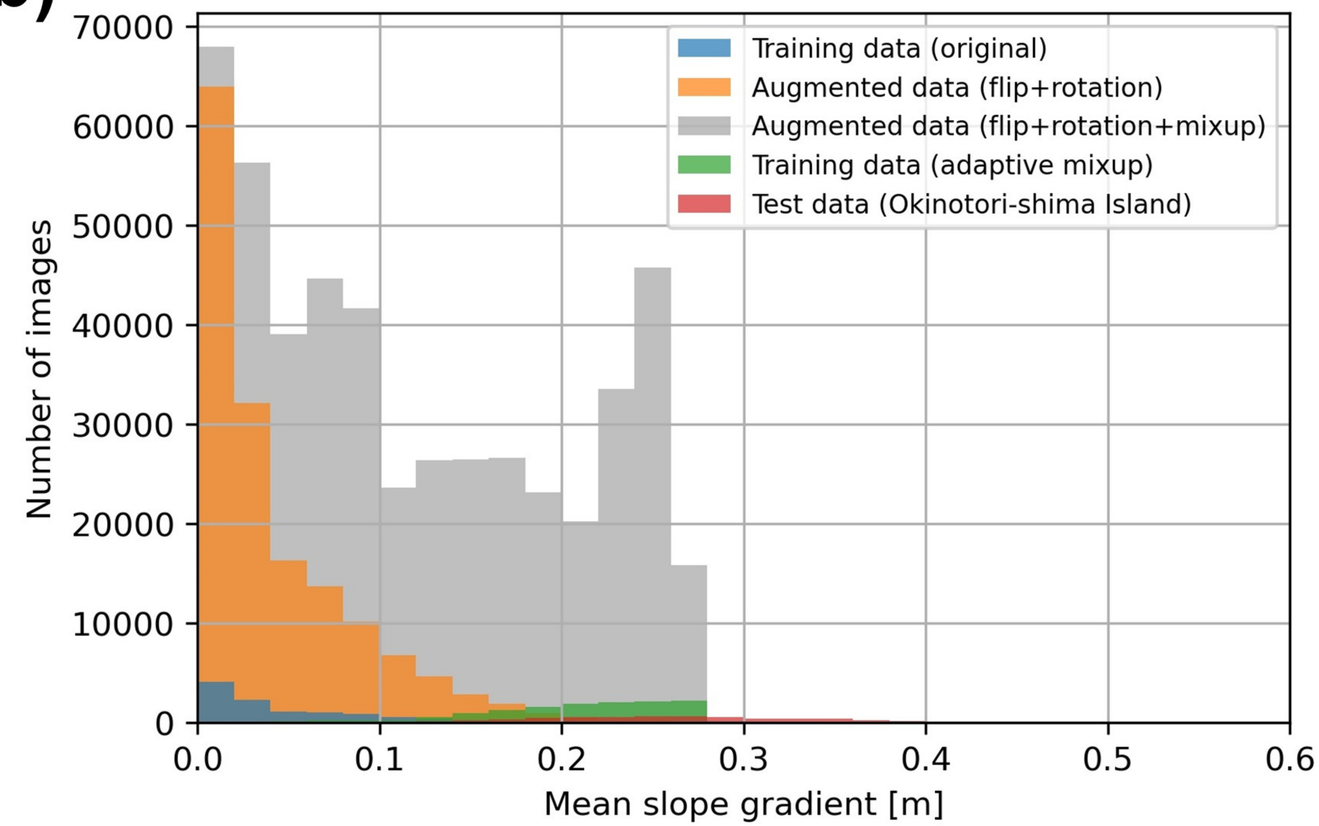

(c)

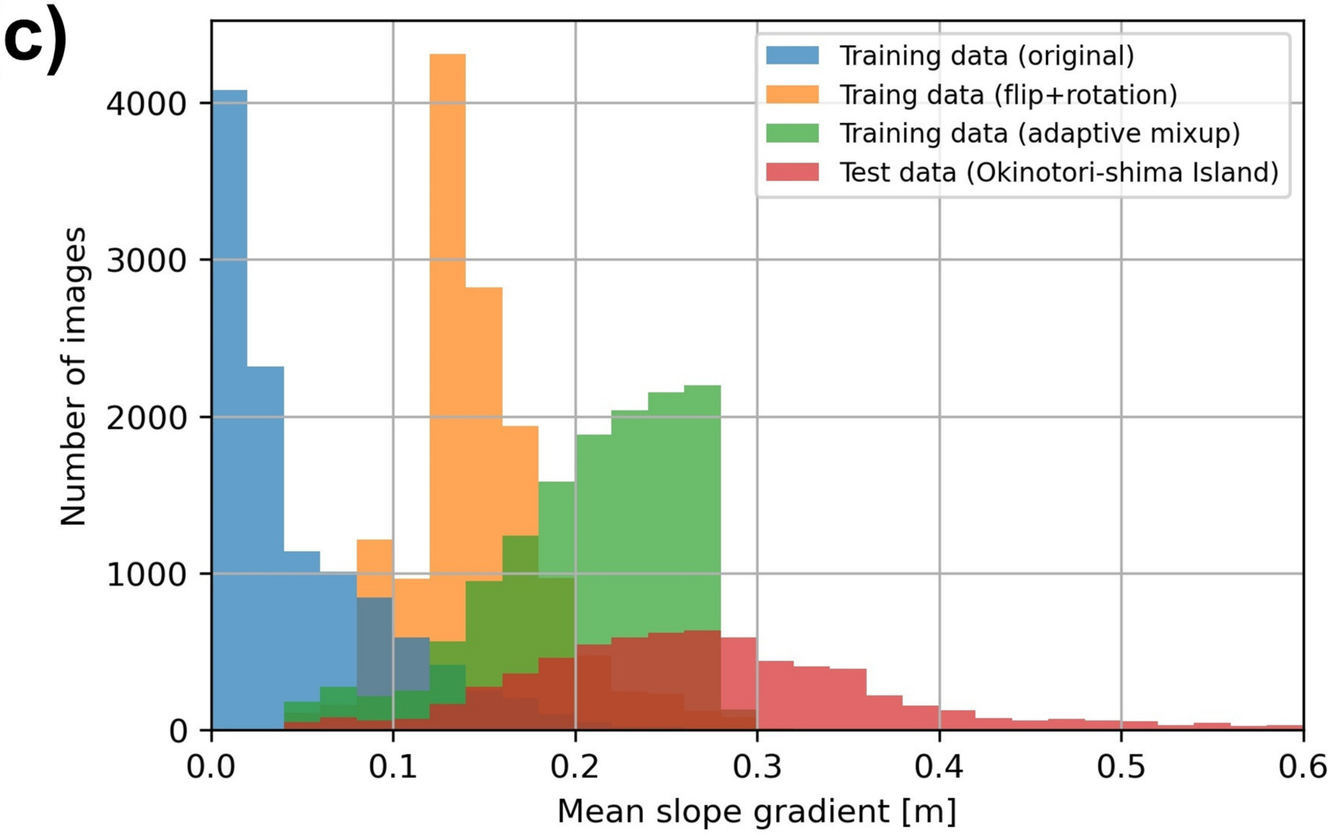

Figure 4.

(a)

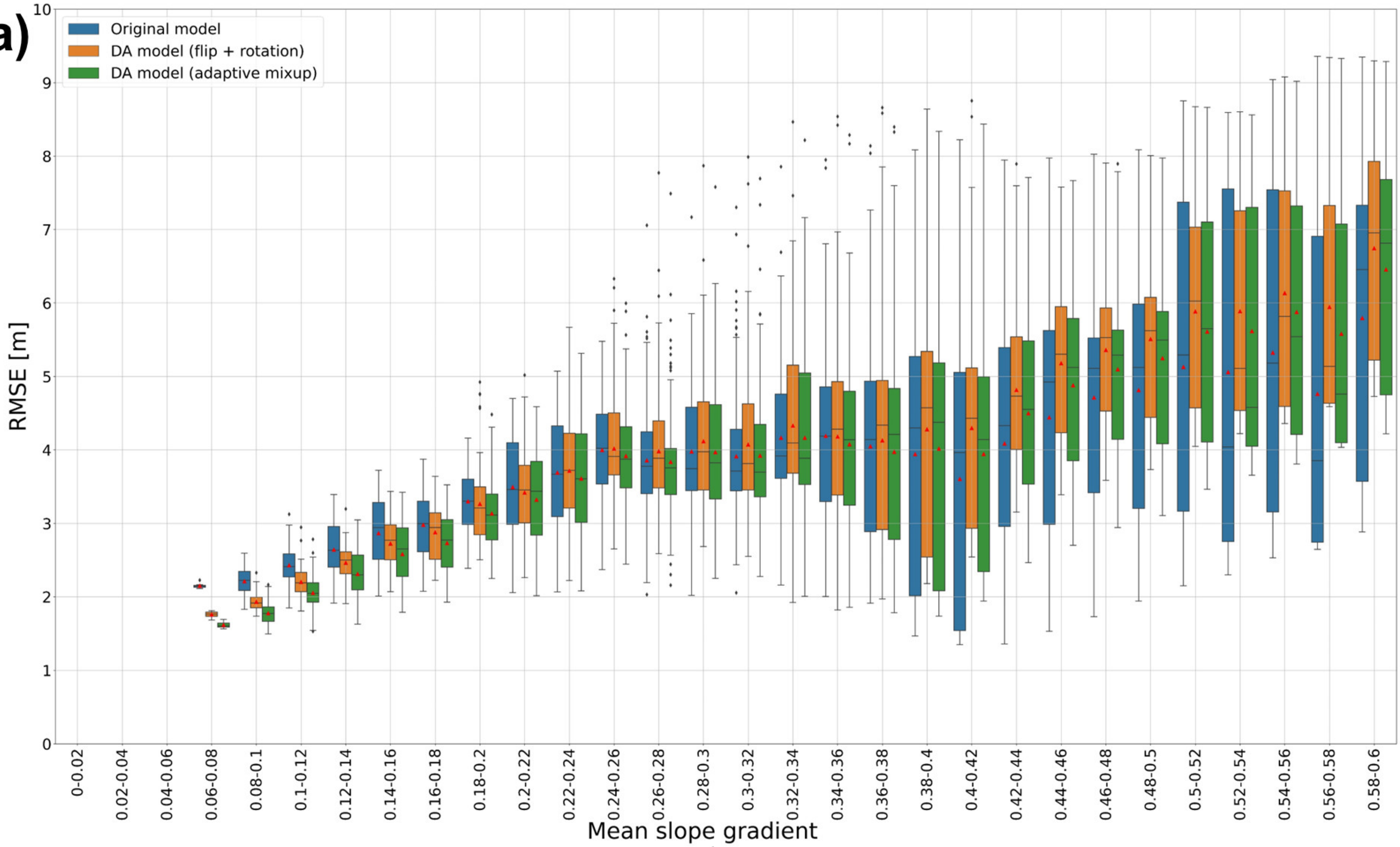
Original model
DA model (flip + rotation)
DA model (adaptive mixup)
RMSE [m]
0
1
2
3
4
5
6
7
8
9
10
0-0.02
0.02-0.04
0.04-0.06
0.06-0.08
0.08-0.1
0.1-0.12
0.12-0.14
0.14-0.16
0.16-0.18
0.18-0.2
0.2-0.22
0.22-0.24
0.24-0.26
0.26-0.28
0.28-0.3
0.3-0.32
0.32-0.34
0.34-0.36
0.36-0.38
0.38-0.4
0.4-0.42
0.42-0.44
0.44-0.46
0.46-0.48
0.48-0.5
0.5-0.52
0.52-0.54
0.54-0.56
0.56-0.58
0.58-0.6
Mean slope gradient

(b)

Original model
DA model (flip + rotation)
DA model (adaptive mixup)
PSNR [dB]
50.0
52.5
55.0
57.5
60.0
62.5
65.0
0-0.02
0.02-0.04
0.04-0.06
0.06-0.08
0.08-0.1
0.1-0.12
0.12-0.14
0.14-0.16
0.16-0.18
0.18-0.2
0.2-0.22
0.22-0.24
0.24-0.26
0.26-0.28
0.28-0.3
0.3-0.32
0.32-0.34
0.34-0.36
0.36-0.38
0.38-0.4
0.4-0.42
0.42-0.44
0.44-0.46
0.46-0.48
0.48-0.5
0.5-0.52
0.52-0.54
0.54-0.56
0.56-0.58
0.58-0.6
Mean slope gradient

Figure 5.

(a)

20°28'
20°27'
20°26'
20°25'
20°24'
20°23'
20°22'
20°21'

136°01' 136°02' 136°03' 136°04' 136°05' 136°06' 136°07' 136°08' 136°09'

PSNR (original) - PSNR (adaptive mixup)[dB]

20
15
10
5
0
−5
−10
−15
−20

(b)

20°28'
20°27'
20°26'
20°25'
20°24'
20°23'
20°22'
20°21'

136°01' 136°02' 136°03' 136°04' 136°05' 136°06' 136°07' 136°08' 136°09'

Mean slope gradient

0.6
0.5
0.4
0.3
0.2
0.1
0.0